Titre: Title:	The role of pore size and mechanical properties on the accumulation, retention and distribution of F98 glioblastoma cells in macroporous hydrogels
Auteurs: Authors:	Lisa Delattre, Sahar Naasri, Angela Giraldo Solano, Hélène Therriault, Simon Bergeron-Fortier, Vaiana Moreau, Benoît Liberelle, Gregory De Crescenzo, Marc-Antoine Lauzon, Nathalie Faucheux, Benoit Paquette, & Nick Virgilio
Date:	2024
Type:	Article de revue / Article
Référence: Citation:	Delattre, L., Naasri, S., Solano, A. G., Therriault, H., Bergeron-Fortier, S., Moreau, V., Liberelle, B., De Crescenzo, G., Lauzon, M.-A., Faucheux, N., Paquette, B., & Virgilio, N. (2024). The role of pore size and mechanical properties on the accumulation, retention and distribution of F98 glioblastoma cells in macroporous hydrogels. Biomedical Materials, 19(4), 045041 (18 pages). https://doi.org/10.1088/1748-605x/ad581b

The role of pore size and mechanical properties on the accumulation, retention and distribution of F98 glioblastoma cells in macroporous hydrogels

IOP Publishing Biomed. Mater. 19 (2024) 045041 https://doi.org/10.1088/1748-605X/ad581b

Biomedical Materials

OPEN ACCESS

RECEIVED
29 February 2024

REVISED
10 June 2024

ACCEPTED FOR PUBLICATION
13 June 2024

PUBLISHED
26 June 2024

PAPER

The role of pore size and mechanical properties on the accumulation, retention and distribution of F98 glioblastoma cells in macroporous hydrogels

Lisa Delattre[1,5], Sahar Naasri[2,5], Angela Giraldo Solano[2,5], Hélène Therriault[2], Simon Bergeron-Fortier[1], Vaiana Moreau[1], Benoît Liberelle[3], Gregory De Crescenzo[3], Marc-Antoine Lauzon[4], Nathalie Faucheux[4], Benoit Paquette[2,*] and Nick Virgilio[1,*]

[1] Department of Chemical Engineering, Research Center for High Performance Polymer and Composite Systems (CREPEC), Polytechnique Montréal, Montréal H3C 3A7 Québec, Canada
[2] Center for Research in Radiotherapy, Department of Nuclear Medicine and Radiobiology, Faculty of Medicine and Health Sciences, Université de Sherbrooke, Sherbrooke J1H 5N4 Québec, Canada
[3] Department of Chemical Engineering, Polytechnique Montréal, Montréal H3C 3A7 Québec, Canada
[4] Department of Chemical and Biotechnological Engineering, Faculty of Engineering, Université de Sherbrooke, Sherbrooke, J1K 2R1 Sherbrooke, Québec, Canada
[5] These authors contributed equally.
[*] Authors to whom any correspondence should be addressed.

E-mail: benoit.paquette@usherbrooke.ca and nick.virgilio@polymtl.ca

Keywords: sodium alginate, macroporous hydrogels, cell accumulation, pore size, compression modulus, glioblastoma

Supplementary material for this article is available online

Abstract

Glioblastoma (GBM) accounts for half of all central nervous system tumors. Once the tumor is removed, many GBM cells remain present near the surgical cavity and infiltrate the brain up to a distance of 20–30 mm, resulting in recurrence a few months later. GBM remains incurable due to the limited efficiency of current treatments, a result of the blood-brain barrier and sensitivity of healthy brain tissues to chemotherapy and radiation. A new therapeutic paradigm under development to treat GBM is to attract and accumulate GBM cells in a cancer cell trap inserted in the surgical cavity after tumor resection. In this work, porous gels were prepared using porous polylactide molds obtained from melt-processed co-continuous polymer blends of polystyrene and polylactide, with an average pore size ranging from 5 μm to over 500 μm. In order to efficiently accumulate and retain GBM brain cancer cells within a macroporous sodium alginate-based hydrogel trap, the pores must have an average diameter superior to 100 μm, with the best results obtained at 225 μm. In that case, the accumulation and retention of F98 GBM cells were more homogeneous, especially when functionalized with RGD adhesion peptides. At an alginate concentration of 1% w/v, the compression modulus reaches 15 kPa, close to the average value of 1–2 kPa reported for brain tissues, while adhesion and retention were also superior compared to 2% w/v gels. Overall, 1% w/v gels with 225 μm pores functionalized with the RGD peptide display the best performances.

1. Introduction

Glioblastoma (GBM) accounts for half of all central nervous system tumors. The median survival time following tumor resection and treatment is of 12–14 months in the adult population, with a 5 year survival rate ranging from 1% to 14% and declining steeply with age [1–3]. GBM cells express a highly invasive phenotype [4, 5]. Consequently, many GBM cells remain present near the surgical cavity after tumor resection, while others have infiltrated the brain up to a distance of 20–30 mm where 80% of tumor recurrences occur. As a result, treatments are planned to expose a large volume of the brain to significant doses of chemotherapeutic drugs and radiotherapy.

Current treatments have limited efficiency due to the blood-brain barrier, restricting the use of intravenous chemotherapeutic drugs [6]. In addition, healthy brain tissues are often more sensitive than GBM cells to radiotherapy, limiting the radiation dose that can be delivered [7]. The current treatment consists in a combination of these last two approaches, with the use of temozolomide (TMZ) as an adjuvant drug increasing the sensitivity of GBM cells to radiation treatments [8]. The sensitivity of neuronal cells and GBM cells to TMZ was determined with GBM tumorspheres obtained with GBM cells isolated from patients. The half-maximal inhibitory concentration (IC50) for TMZ was more than 2-fold higher for most of the tested GBM cells, compared to HNPC and NS5 human neural stem cells. The lethal dose of radiation to eliminate 50% of the cancer cells (LD50) was superior to 60 Gy for 43.6% of the GBM tumorspheres. In contrast, the LD50 for human neural stem cells was between 10 and 12 Gy [7]. Consequently, most patients do not receive a dose of TMZ or radiotherapy that would significantly eliminate GBM cells. In addition, the high sensitivity of healthy brain tissue under the current treatments can lead to necrosis and alter cognitive functions [9]. As a complementary treatment, the Gliadel Wafer system can also be placed on-site after tumor resection, delivering carmustine, a chemotherapeutic drug [10]. However, mixed clinical results are obtained and various complications arise [11]. Actually, no successful treatment for GBM exists [12].

An emerging therapeutic alternative consists in using a GBM cancer cell trap that would attract, accumulate and retain GBM cells in a confined location, followed by localized stereotaxic radiotherapy to eliminate them. By eliminating GBM cells this way, healthy tissues would receive a much lower radiation dose, which should help limit cognitive losses, resulting in an improved quality of life. Autier *et al* have demonstrated the feasability of such an approach with F98 GBM cells, using a bacterial cellulose membrane acting as a trap accumulating GBM cells [13]. Recently, our team has developed a macroporous hydrogel cancer cell trap composed of sodium alginate (SA) and chitosan (CHI), functionalized with the RGD adhesion peptide [14, 15], and displaying mechanical properties comparable to those of brain tissue (compression modulus $\approx$ 1–10 kPa) [16–18]. These macroporous gels are fabricated by a template-based technique, using porous polylactide (PLA) molds obtained from melt-processed co-continuous polymer blends of PLA and polystyrene (PS) [19]. Briefly, the average pore diameter can be tuned over a range of 1–1000 μm, while maintaining nearly full pore interconnectivity. This approach is compatible with numerous gel chemistries, including both physical and chemical crosslinking strategies [19, 20]. F98 GBM cells were able to infiltrate and accumulate in these gels due to the presence of fully interconnected macropores ranging in average diameter from 300 to 600 μm [14, 15]. The concept is to implant the hydrogel in the surgical cavity after tumor removal. The controlled release of a chemoattractant, such as CXCL12, will attract the remaining GBM cells within the hydrogel via a network of interconnected pores. Once accumulated and retained inside the gel, the GBM cells will be irradiated by stereotaxic radiosurgery. A higher dose of radiation can thus be locally delivered to the GBM cells, while preserving the healthy brain tissue at the periphery of the trap.

Porosity, including the average pore diameter and pore interconnectivity, has an impact on the cellular behavior inside a 3D biomaterial, including porous hydrogels. However, experimental data establishing a relationship between pore size and pore interconnectivity, with the capacity of cells to penetrate and accumulate in 3D porous hydrogels (and 3D biomaterials in general), remain relatively scarce—due in part to the capacity of fabricating well-controlled 3D porous gels in sufficient numbers. Chiu *et al* [21] demonstrated *in vitro* that the vascularization rate in porous polyethylene glygol hydrogels increased with pore size, and took place throughout the entire material, up to a maximum tested diameter of 150 μm. The invasion area was however twice as important in gels comprising 100–150 μm pores, compared to gels with 25–50 μm pores. For *in vivo* experiments, the process was limited to the external surface for gels with 25–50 μm pores, while it occurred throughout the whole volume for larger pores. This indicates that there is a minimum pore size value allowing cell migration inside a soft porous hydrogel.

Cellular behavior is also impacted by the mechanical properties of biomaterials, such as stiffness and surface texture. For example, it has been reported that cellular migration is reduced on stiffer surfaces of 2D substrates due to more stable focal adhesion points [22, 23]. However, reports analyzing both the impacts of pore size and gel stiffness are scarce. Lang *et al* [24] reported higher MDA-MB 231 (human epithelial breast cancer cells) cell invasion in stiffer crosslinked collagen gels, when the pore size was superior to 5 μm. However, the opposite trend was observed under this threshold value.

In this work, we assess the effects of both pore size and gel compression strength on the accumulation, retention and distribution of GBM cells inside sodium alginate-based macroporous hydrogels, functionalized with RGD adhesion peptides.

2. Materials and methods

2.1. Materials

Polylactic acid Ingeo™ 4032D was supplied by NatureWorks (PLA, melt flow index = 7 g/10 min

@ 210 °C/2.16 kg, ρ (200 °C) = 1.11 g cm^{-3}, melting temperature Tm = 169 °C), while polystyrene MC3650 was obtained from Americas Styrenics (PS, melt flow index = 13.0 g/10 min @ 200 °C/5 kg, ρ (200 °C) = 0.97 g cm^{-3}). Sodium alginate (SA, grade IL-6 G) was provided by the Kimica Corporation (M/G ratio = 0.5, η = 30–60 mPa s (1%), Mw = 67 000 ± 8000 g mol^{-1} and polydispersity index PDI = 2.1, measured by GPC [15]).

Cyclohexane and chloroform were ACS-grade chemical reagents. Calcium chloride ($CaCl_2$), 1-(3-dimethylaminopropyl)-3-ethylcarbodiimide hydrochloride (EDC, 99+% purity), *N*-hydroxysuccinimide (NHS, 98% purity) and sodium azide S2002 (⩾99.5%) were purchased from Sigma-Aldrich. The CGGRGDS peptide (RGD, cysteine-terminated) was provided by EZbiolab (98%, N-terminal acetyl, C-terminal amide, New Jersey, USA). N-ε-maleimidocaproic acid hydrazide (EMCH) was provided by ThermoFisher Scientific. All aqueous solutions were prepared with MilliQ water (18.2 MΩ·cm; total organic compounds (TOC) ⩽ 5 ppb). The glassware was cleaned by overnight immersion in a bath of KOH-saturated isopropyl alcohol, followed by intensive rinsing with Milli-Q water. All tools were cleaned with MilliQ water and ethanol 70% v/v before use.

2.2. Preparation of macroporous polylactide (PLA) molds

The full procedure is described in detail in previous publications [14, 15]. Briefly, immiscible blends of PS and PLA (50/50 wt%, in order to obtain a co-continuous morphology) were prepared using an AG 34 mm Leistritz co-rotating twin-screw extruder at 190 °C, with a residence time of 2–3 min. The extruded rods were then quenched in cold water to freeze-in the morphology. Next, using a hot press, the rods were annealed at 190 °C (for 5, 10, 20, 30, 45 or 60 min) to let the morphology coarsen, followed by rapid quenching in water to freeze the morphology again. The annealed rods were then trimmed into cylinders (diameter = 1 cm, height = 0.6 cm) by computerized numerical control (CNC) machining with a Genmitsu 3020-PRO MAX Routeur instrument, and the PS phase was selectively extracted with cyclohexane using a soxhlet apparatus. The resulting porous PLA molds were finally dried overnight in a vacuum oven at 40 °C.

2.3. Preparation and modification of sodium alginate (SA) with RGD peptide

SA powder was dissolved in warm water (1% w/v) and filtered with PROGENE® Vacuum Filtration Units (0.22 µm, polyethersulfone membrane, Ultident Scientific, Saint-Laurent, Québec, Canada), and was finally freeze-dried. The resulting filtered SA was then stored at 4 °C.

2.3.1. RGD peptide grafting

Filtered SA was first dissolved in MilliQ water (1% w/v). Aqueous aliquots of 0.1 M NHS (3.5 µl) and 0.4 M EDC (1 µl), initially stored at −80 °C, were thawed and added to 40 mL of SA solution. The solution was then stirred on an orbital plate shaker for 20 min at room temperature (RT), and a 10 mM aliquot of EMCH dissolved in DMSO (17.5 µl, initially stored at −80 °C) was thawed and added to the solution, followed by 60 min of additional shaking at RT on the orbital shaker. Next, 56.9 µl of a 2 mg ml^{-1} RGD solution (stored at −80 °C and thawed before use) was added, corresponding to 3.5 × 10^{-7} mol of cysteine-terminated peptide per 400 mg of SA. The resulting solution was stirred for 20 h, filtered five times using centrifugal Amicon Ultra-15 filter units with a 10 kDa membrane (Merck Millipore, Tullagreen, Ireland) to eliminate any residual free peptide and reagents. The resulting RGD-grafted SA (SA-RGD) was freeze-dried and stored at 4 °C.

2.4. Preparation and characterization of macroporous SA hydrogels

2.4.1. Preparation of macroporous hydrogels

Four different precursor gelling solutions were prepared using milliQ water: (1) 1% or 2% w/v of pristine filtered SA, and (2) 1% or 2% w/v of SA-RGD. Next, porous PLA molds were individually deposited in 15 mL falcon tubes, and 3 mL of precursor gelling solution were poured in the tubes to fully cover each mold. The tubes (without lids) were deposited in a custom-built injection system applying pressure-vacuum cycles, and three to four vacuum/high pressure cycles under N_2 were applied, or until most of the trapped air bubbles were expelled from the molds, ensuring that the pores were filled with the gelling solution. The molds were taken out and gently wiped to remove any excess of solution, and they were deposited in a 0.22 µm filtered 4% w/v $CaCl_2$ solution overnight to complete the gelation process.

Next, the PLA molds filled with the gels were transferred into vials containing 10 ml of chloroform. The vials were placed onto a shaker plate set at 60 RPM to extract the PLA phase, and the chloroform was changed every two or three days (four solvent changes in total), until the PLA phase was completely extracted, in order to obtain nearly transparent macroporous SA hydrogels. The gels were then rinsed in water for two days (two water changes in total) to eliminate the residual chloroform, and they were then stored at 4 °C in a 0.22 µm filtered 4% w/v $CaCl_2$ solution, with the addition of 6 droplets of a 5% w/v sodium azide solution per 500 mL of 4% $CaCl_2$ solution, to prevent bacterial proliferation, for gels destined to cellular assays.

2.4.2. Measurement of compression modulus

The unconstrained compression modulus of the macroporous gels filled with water was measured with a Mach-1 mechanical Tester (Biomomentum, Laval, Canada, Actuator A400.25, 150 g load cell) and the Mach-1 Motion software. The diameter of the indenter (2 cm) was larger compared to the diameter of the gels (1 cm). For each gel, the precise dimensions (diameter D_0 and height L_0) were measured with a micrometer right before the tests.

Briefly, the procedure consisted first in finding contact with the gel (piston speed = 25 µm s^{-1}, contact finding criteria: 0.25 g). Next, a first pre-compression (piston speed = 25 µm s^{-1}), corresponding to a displacement of 50 µm (strain $\varepsilon \cong 0.9\%$), was applied in order to ensure full contact with the surface of the gel. Finally, a second compression of 25 µm (piston speed = 20 µm s^{-1}) was applied to subsequently evaluate the compression modulus. The instrument recorded the displacement (ΔL, in µm) and the applied load (m, in kg) at an acquisition rate of 0.1 s^{-1}. The applied strain ε (%) and recorded stress σ (Pa) as a function of time were calculated with equations (1) and (2):

$$\varepsilon = \frac{\Delta L}{L_0} \tag{1}$$

$$\sigma\,(\text{kPa}) = \frac{\text{Force}}{\text{Surface area}} = \frac{m \cdot g}{\frac{\pi D_0^2}{4}} \tag{2}$$

with g being the standard gravity and D_0 the gel diameter.

The compression stress σ was plotted as a function of ε. The data were then fitted with a linear regression to obtain the slope corresponding to the compression modulus. Seven macroporous gels were tested per formulation, and the average modulus and standard deviation were calculated. In all cases, ε_{max} was always inferior to 1.5% and the recorded stress varied linearly with ε (see figure S1). For such small strain values, no variation of the diameter was observed by visual inspection. We then considered the surface area as constant when calculating the applied stress with equation (2).

2.5. Microstructure characterization of PLA molds and SA hydrogels by x-ray microtomography

MicroCT images of macroporous PLA molds, and of a 2% w/v SA macroporous hydrogel (with the pores emptied of water using Kimwipe papers), were obtained with a Zeiss Xradia 520 Versa instrument operated at 40 kV and 75 µA. First, a Noise Reduction Filter (NRF) was applied with the Scout-and-scan Control System Reconstructor software to remove ring artifacts. The resulting files were then post-processed with the Dragonfly software. The first step was to modulate the image contrast to obtain a black and white reconstruction—pores are black and PLA phase (or gel phase) is white. Next, each domain (PLA, gel, or pores) was selected to create masks. Finally, a cylindrical cut was made to get rid of the sample holder and of the outside environment. The thickness mesh of each domain was obtained using a built-in algorithm, yielding the average domain size and domain size distributions. The pore surface was also determined using a built-in algorithm, and was divided by the sample volume to give the specific pore surface.

2.6. F98 fluorescent cell generation and culture

F98 cells of murine origin were provided by the American Type Culture Collection (Manassas, VA, USA). Cells were cultured in DMEM media supplemented with 10% fetal bovine serum (FBS), 44 mM sodium bicarbonate, 2 mM l -glutamine, and an antibiotic mixture consisting of penicillin (100 U ml^{-1}) and streptomycin (100 µg ml^{-1}). The cells were incubated at 37 °C in a humidified environment in the presence of 5% CO_2. The lentiviral vector pCDH-CMV-mCherry-T2A-Puro (Addgene Catalog#72264, Watertown, MA, USA) was used to introduce the mCherry fluorescence marker into F98 cells [25]. Cells expressing the mCherry marker were incubated for 10 d in DMEM media containing 2.5 µg ml^{-1} of puromycin. The expression of mCherry by F98 cells was confirmed by observation with a Leica DM-IRBE fluorescence microscope. The doubling time was determined by plating 10^3 cells per well in 96-well plates and the kinetic of cell growth was then measured daily by fluorescence (λ_{ex} = 530 nm, λ_{em} = 590 nm) with a microplate reader (HT Synergy, Bio-Tek Instrument,Winooski, VT, USA).

2.7. Sterilisation of macroporous hydrogels

After depositing the macroporous hydrogels in 96- or 48-well plates, 70% (v/v) ethanol was added for 10 min. The hydrogels were next rinsed with distilled water and incubated overnight in a solution of $CaCl_2$ 4% w/v diluted in phosphate buffered saline (PBS). After 24 h, the hydrogels were washed twice with DMEM media without additives, supplemented only with 0.1% w/v bovine serum albumin (BSA) for 20 min. Finally, the hydrogels were stored in DMEM + BSA media at 4 °C.

2.8. F98 cell accumulation and retention assays in macroporous hydrogels

Both the accumulation and retention of the F98 cells into the macroporous hydrogels were determined using similar methods. The sterilized macroporous hydrogels were placed in 96-well plates. F98 mCherry cells (1×10^6 cells) were added dropwise to the upper surface of each hydrogel, then placed in the incubator at 37 °C and 5% CO_2. After 5 h of incubation, the hydrogels were inserted into new 96-well plates, containing 100 µl of DMEM media per well in order to

remove the F98 cells remaining at the external surface of the hydrogels. The number of cells accumulated in the hydrogels was measured next by fluorescence ($\lambda_{ex} = 530$ nm, $\lambda_{em} = 590$ nm) with a microplate reader (HT Synergy) calibrated with a standard curve.

The hydrogels were then returned to the incubator for 24 h in order to let the F98 cells adhere to the pores in the hydrogels. The hydrogels were then transferred in a migration chamber (TC-Insert, Sarstedt, Catalog#83.3922.800, Nümbrecht, Germany) connected to a syringe to carry out a stringent washing [15]. Briefly, F98 cells that did not sufficiently adhered to the hydrogels were removed with 300 µl of DMEM passing through the hydrogels. The number of F98 cells retained by the hydrogels was determined by fluorescence as described previously.

2.9. Distribution of F98 cells into the hydrogels

The distribution of F98 cells in the hydrogels was determined by epifluorescence microscopy combined with image analysis. F98 mCherry cells (0.5×10^6 cells/ hydrogel) were added dropwise onto the upper surface of the hydrogels. After 24 h of incubation, the hydrogels were placed in 24-well plates and fixed with a solution of paraformaldehyde (PFA) 3% w/v for 15 min at RT. In new plates, the hydrogels were next washed with DMEM media for 5 min twice. Hydrogels were placed once again in a new plate in the presence of 1% BSA (blocking agent) for 30 min at RT and then washed twice with DMEM media for 2 min. Finally, the cells were stained by incubating the hydrogels in the presence of a solution of Rhodamine-phalloidin 2105 247 (actin cytoskeleton, red channel) (1:100) and Hoechst 33 342 (nuclei, blue channel) at a concentration of 5 µg ml^{-1} in 0.1% w/v BSA/DMEM red phenol free for 30 min, at RT and in the dark. Afterwards, the hydrogels were washed twice with DMEM media for 2 min and then kept in PBS at 4 °C.

The distribution of F98 cells inside the hydrogels was determined at 5 different levels (L), starting at about 1 mm deep from the superior face of the hydrogels (referred as L1), to about 4.5 mm deep (L5) (total hydrogel thickness of 5 mm) using the EVOS™ FL Auto Imaging System epifluorescence microscope (Life Technologies), as described previously [15].

2.10. Statistical analysis

Results are expressed as the mean ± standard deviation of 2–4 experiments performed in triplicate. Statistical analyses were performed using two ways analysis of variance (ANOVA). A value of $p < 0.05$ was considered to be statistically significant. $^{*}p < 0.05$, $^{**}p < 0.01$, $^{***}p < 0.001$, $^{****}p < 0.0001$. The Benjamini, Krieger and Yekutieli method was used as false discovery rate control with a Q value of 0.05.

3. Results

3.1. Morphology analysis of PLA molds and macroporous hydrogels

Figure 1(A) displays the porous PLA molds as a function of quiescent annealing time t_{anneal} (from left to right: 5 min to 60 min). The porosity becomes apparent after 30 min of annealing time and continues to coarsen as t_{anneal} is prolonged. Figure 1(B) next displays the resulting porous SA gels once the PLA molds are removed by selective extraction (1% SA on top, 2% SA at the bottom). The effect of increasing pore size on gel turbidity is also apparent, as they become more transparent as pore size increases. No obvious difference is observed between the two SA concentrations. The gels are slightly smaller compared to the PLA molds, as the scale bars show. The dimensions are also slightly distorted for the 1% SA gels at 5 and 10 min of annealing times, since they are softer and more difficult to manipulate.

Figure 2 next shows that the microstructure of porous PLA molds coarsens significantly as a function of annealing time, as revealed by x-ray microCT analysis. The porosity remains fully interconnected throughout the material, for all annealing times (see also 3D reconstructions in figure S2). While the morphology is homogeneous up until 20 min of annealing times (Figure 2(A)–(C)), it becomes gradually more heterogeneous as coarsening and phase separation progress (Figure 2(D)–(F)). Table 1 presents the morphological features of the polymer blends as a function of t_{anneal}, for both the PLA and PS polymer phases. The pore size distributions are presented in figure S3.

Following image analysis of the PLA molds, the volume fractions (% of the volume occupied by each component in the blend) of both PLA and PS phases are near 50%, which is close to the 50/50 mass ratio fed to the extruder (note that the porosity of the PLA molds is generated by extracting the PS phase). Local composition fluctuations can also occur when using melt-extrusion to process polymer blends. The average PLA domain diameter (i.e. thickness of the PLA domains) ranges from 7 ± 1 µm after 5 min of annealing time, to 577 ± 315 µm after 60 min, with the specific interfacial area S (the area of the PS/PLA interface per unit volume of blend) decreasing from nearly 2900 cm^{-1} to 24 cm^{-1}. These results are consistent with previously published results [19].

Figure 2(G) shows that both average domain diameters (or domain thicknesses) for PLA and PS (d_{PLA} and d_{PS}) increase slowly for the first 10 min, which is due to the thermal inertia. Coarsening then accelerates and increases nearly linearly with time, until it slows down again around 45 min. Such a linear increase, followed by a slower increase or

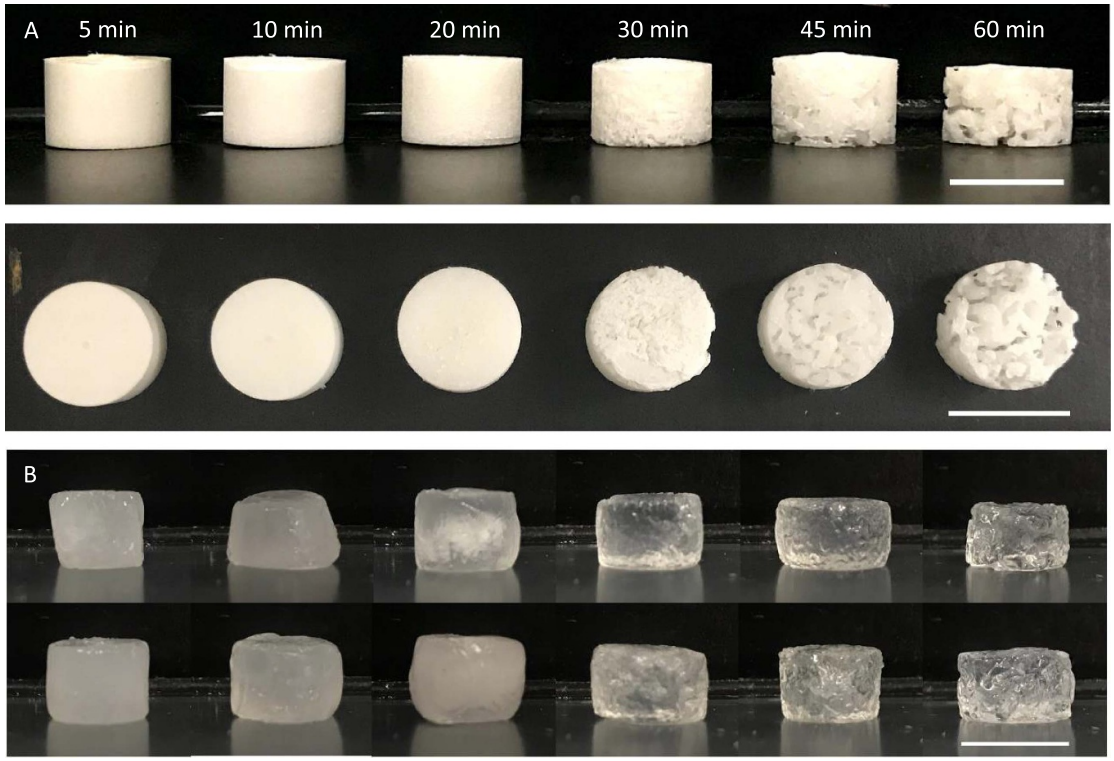

Figure 1. (A) Lateral and top views of polylactide (PLA) macroporous polymer molds, with corresponding annealing times, obtained after selective PS extraction. The porosity is apparent for gels prepared with PLA molds initially annealed for 30 min or longer. (B) Lateral views of resulting macroporous sodium alginate (SA) hydrogels (top row: 1% SA (w/v); bottom row: 2% SA (w/v)). For (A) and (B), from left to right: quiescent annealing times of 5, 10, 20, 30, 45 and 60 min (also indicated in (A)). The scale bar corresponds to 1 cm.

nearly constant plateau value, have also been reported previously [26, 27]. This increase in domain diameter is driven by the PLA/PS interfacial tension (5.8 mN m^{-1} [28]), which is a measure of the lack of affinity between the two polymers—the higher the interfacial tension, the faster the coarsening process. The coarsening rate however decreases as the viscosity of the polymer phases increases, providing a way to control the process. This increase in domain diameter or thickness is also accompanied by a decrease in the specific interfacial area *S*, i.e. the area at the PLA/PS interface, as demonstrated previously [19, 26].

The porosity features of the PLA molds (average pore diameter, volume fraction, etc.) correspond to the PS phase microstructural parameters, since extracting the PS phase yields the porosity. In contrast, the porosity features of the porous SA gels correspond to the PLA phase, since the PLA is extracted in order to yield the macroporous SA gels. However, directly visualizing the porosity within the gels remains difficult—especially at short annealing times. Water needs to be removed from the pores to enhance the contrast between the gel phase and the pores when using microCT, which often results in gel shrinking and, ultimately, collapse of the network of pores at small pore sizes. Still, previous works have demonstrated that the network of pores within the gels closely match the microstructure of the porogen (extracted) polymer phase, in this case PLA [15, 19].

Figure 3 shows a visual comparison between a PLA mold after 45 min of annealing time, and the resulting macroporous hydrogel. The microstructural parameters are presented in table 2.

Visual inspection shows that the microstructures are comparable in scale. First, we must keep track of how the PS and PLA phases are gradually replaced to finally obtain macroporous hydrogels. Since the technique is basically a molding approach, the PLA domains (in white) in figure 3(A), for the polymer mold, must be compared to the pores within the hydrogel (in black) in figure 3(B), whereas the PS phase in figure 3(A) (in black, following PS extraction) must be compared to the gel domains (in white) in figure 3(B). The pores in the gel are larger in average compared to the PLA domains of the mold (580 μm VS 487 μm), whereas the opposite trend is observed when comparing the average size of the PS domains in the mold, to the gel domains. The volume fraction associated to the pores in the hydrogel is also higher compared to the PLA phase volume fraction in the mold (the opposite is observed when comparing the PS and gel phases). Accordingly,

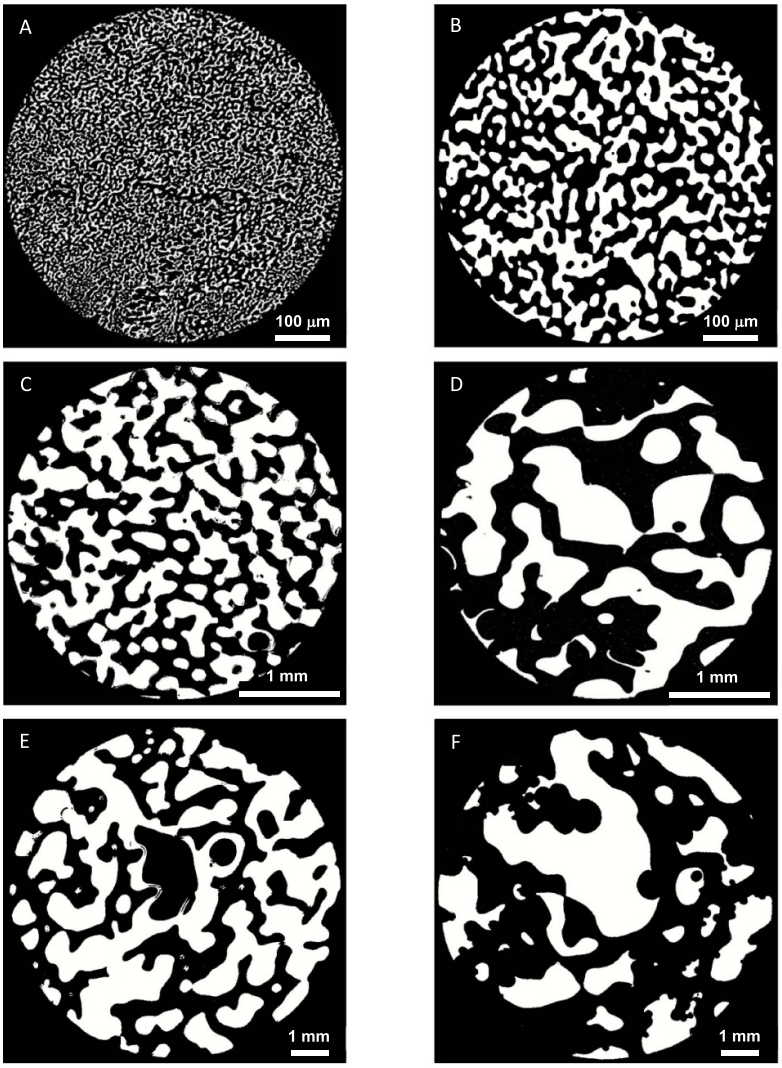

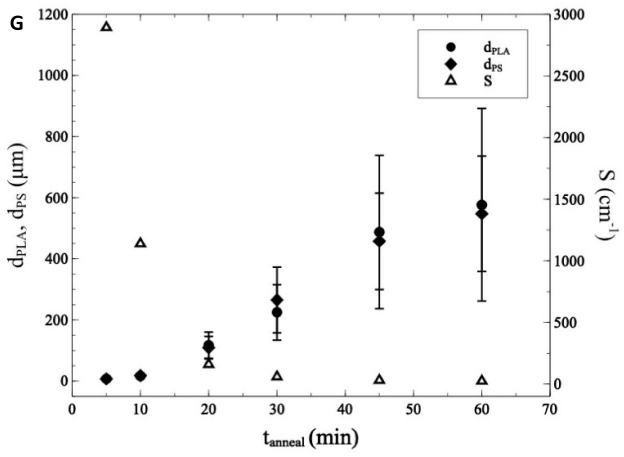

Figure 2. Microstructure of porous PLA molds as revealed by x-ray microCT, as a function of quiescent annealing time. From (A) to (F), annealing times t_{anneal} of 5 (A), 10 (B), 20 (C), 30 (D), 45 (E) and 60 (F) min. The microstructure gradually coarsens as quiescent annealing is prolonged. White domains correspond to PLA, black domains correspond to the pores left by the selective extraction of the PS phase. Note also the different scale bars employed in order to better visualize the microstructure. (G) Average diameter (thickness) of the PS (d_{PS}) and PLA (d_{PLA}) domains in the blend, and specific interfacial area S, as a function of quiescent annealing time t_{anneal}. The data points for the diameters correspond to the average pore size of the distribution ± one standard deviation. The pore size distributions as a function of t_{anneal} are presented in figure S3 in the supporting information file.

Table 1. Microstructural parameters of polymer blends as a function of quiescent annealing time. Note that 3 samples were analyzed for annealing times of 45 and 60 min ($N = 3$). Domain diameter corresponds to the pore size distribution average ± 1 standard deviation.

	PLA phase		PS		
Quiescent annealing time (min)	Volume fraction ϕ_{PLA}	Average domain diameter d_{PLA} (μm)	Volume fraction ϕ_{PS}	Average domain diameter d_{PS} (μm)	Specific interfacial area S (cm^{-1})
5	53	7 ± 1	47	7 ± 1	2892
10	44	16 ± 5	56	18 ± 4	1138
20	47	118 ± 43	53	109 ± 37	160
30	40	225 ± 91	60	265 ± 108	58
45	44 ± 3	487 ± 251	55 ± 3	457 ± 158	30 ± 5
60	47 ± 2	577 ± 315	53 ± 2	548 ± 189	24 ± 2

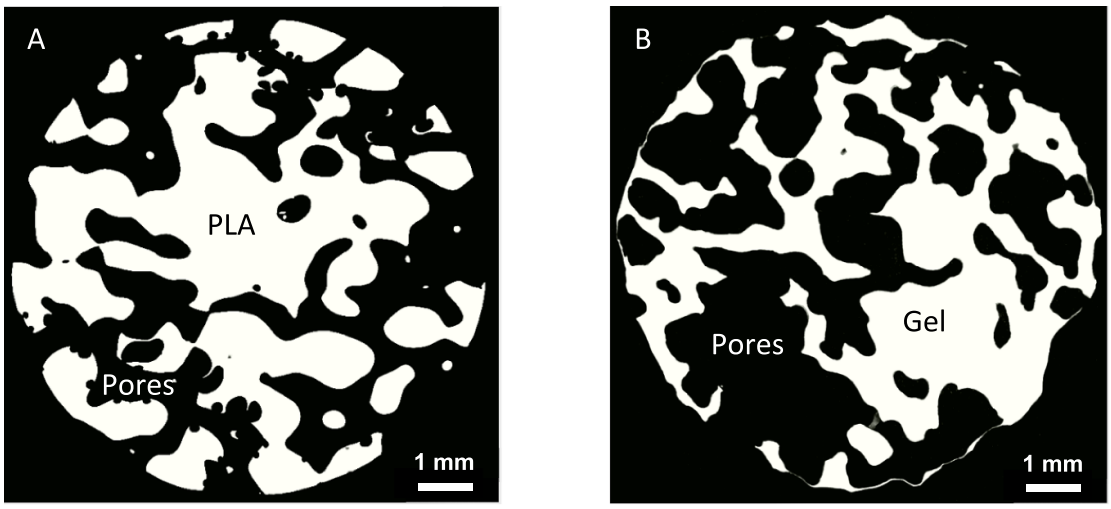

Figure 3. (A) Microstructure of PLA mold (45 min of annealing time) and (B) resulting macroporous gel once the PLA phase is extracted. In (A), white domains = PLA, black domains = porosity left by PS extraction, whereas in (B), white domains = gel phase, black domains = porosity left by PLA selective extraction. The comparison must then be made between the PLA domains in (A) and the porosity in (B), and the PS (pores) domains in (A) and gel phase in (B).

Table 2. Comparison of the microstructural features between a porous PLA mold and porous hydrogel, for an annealing time of 45 min.

Sample ID	Comparison of d_{PLA} in mold and d_{pores} in gel (μm)	Comparison of $d_{PS(Pores)}$ in mold and d_{gel} in gel (μm)	Comparison of ϕ_{PLA} in mold and ϕ_{pores} in gel (vol%)	Comparison of $\phi_{PS(Pores)}$ in mold and ϕ_{gel} in gel (vol%)	Comparison of S between PLA mold and gel (cm^{-1})
Polymer mold	487 ± 251	457 ± 158	45	55	30
Porous gel	580 ± 250	406 ± 188	55	45	26

the specific surface is slightly higher for the PLA mold.

Since the volume difference between the mold and resulting porous gel is negligible as a first approximation (see figure 1), these variations could be explained by two phenomena: (1) syneresis of the gel phase, leading to the expulsion of water contained in the gel phase, with the associated decrease of the gel volume fraction compared to the initial corresponding PS phase, and both a decrease of the average gel domain size and increase in average pore size; (2) the difficulty in fully removing water within smaller pores, which could artificially increase the average diameter of the pores, shifting the pore size distribution to higher values, and decreasing the specific surface area, S. Nevertheless, the gels retain relatively well the microstructure of the molds.

It was not possible to perform such a comparison at a lower pore size, since removing water from the pores proved much more difficult, resulting in gel shrinking and collapse of the porosity. As a result, in the sections that follow, porous gels will be identified using the average diameter (thickness) of the PLA domains of the associated polymer molds.

3.2. Compression properties of macroporous hydrogels

The compression modulus of the porous gels were measured as a function of both SA concentration

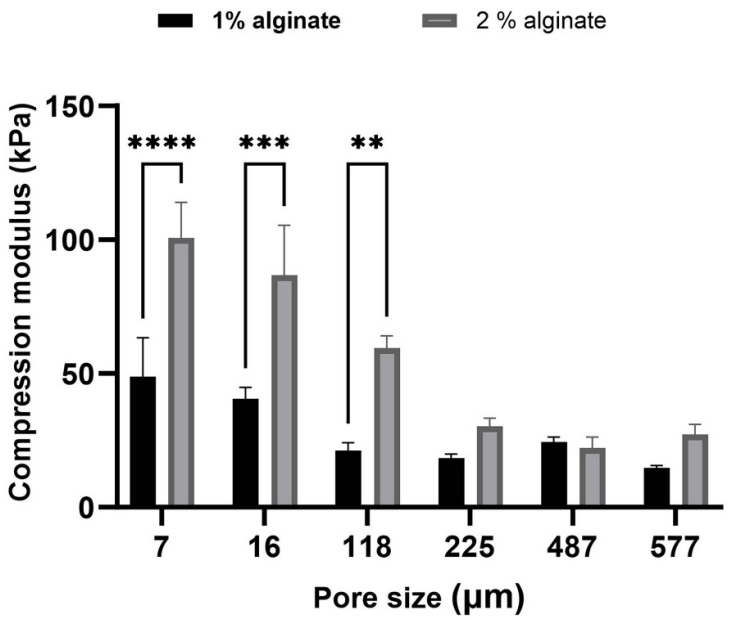

Figure 4. Unconstrained compression modulus of macroporous hydrogels as a function of average pore diameter d_{pores}, and SA concentration. Each value corresponds to the average modulus ± one standard deviation of 7 gels.

(1% or 2% w/v), and average pore diameter—the target being in the range of 1–2 kPa in order to match the modulus of brain tissues [16–18]. The compression modulus, as expected, generally increases as the SA concentration increases, at a given pore size, as figure 4 illustrates. More specifically, increasing the concentration of SA from 1% to 2% nearly doubles the compression modulus value, for all pore sizes, except at 487 µm, for which both values are comparable. Whether it is due to experimental variability or a mistake during gel preparation remains to be verified—however, there is no significant difference in terms of porosity volume fraction for the PLA molds used to prepare these gels, compared to the other pore sizes (table 2).

The compression modulus also generally decreases as pore size increases, for both SA concentrations. From 7 µm to 225 µm, there is a sharp decrease from nearly 100 kPa to 39 kPa at 2% SA (a similar trend is observed at 1% SA, with lower moduli). The modulus remains nearly constant as the average pore size further increases, around 25–40 kPa at 2% SA, and around 15–25 kPa at 1% SA. We found no previous work establishing a relationship between the compression modulus value and the average pore size for porous gels. However, a recent work on poly(methyl methacrylate) foams by Zhang *et al* [29] displayed a similar trend, with the compression modulus sharply decreasing as the pore size increased, at small pore size values, followed by a slower decrease as pore size continued to increase, at larger pore size values. They demonstrated by numerical modeling that at small pore sizes, the stress concentration is more homogeneous and the porous structure is 'self-reinforcing', whereas at larger pore size stress concentrates in the walls or struts, where failure occurs. However, in their work, there is no mention related to the effect of the resistance of water expulsion as compression occurs, which should offer increased resistance as the pore size decreases, and which could have an impact in our work. This will be investigated in a future work.

3.3. Accumulation, retention and distribution of F98 cells in hydrogels

F98 cells expressing the fluorogenic marker mCherry were deposited on the upper surface of the hydrogels, from where they migrated and then adhered to the pores in the hydrogels. The accumulation of F98 cells was determined first by gently washing the hydrogels, whereas adhesion of the cells to the surface of the pores was quantified afterwards following a more stringent washing step, as detailed in section 2.8 and in previous publications [14, 15]. As mentioned at the end of the Introduction, the objective herein was to determine which average pore diameter(s) and SA concentration(s) optimized the accumulation, retention and distribution of F98 cells in the hydrogels, and to evaluate the impact of grafting the RGD adhesion peptide to SA.

3.3.1. Cell accumulation

Hydrogels comprising smaller pores have a larger available adhesion surface for GBM cells, as compared to gels with larger pores (as table 1 and figure 1 demonstrate), which should promote cell accumulation. However, tortuosity also increases at a smaller pore diameter which, when combined with F98

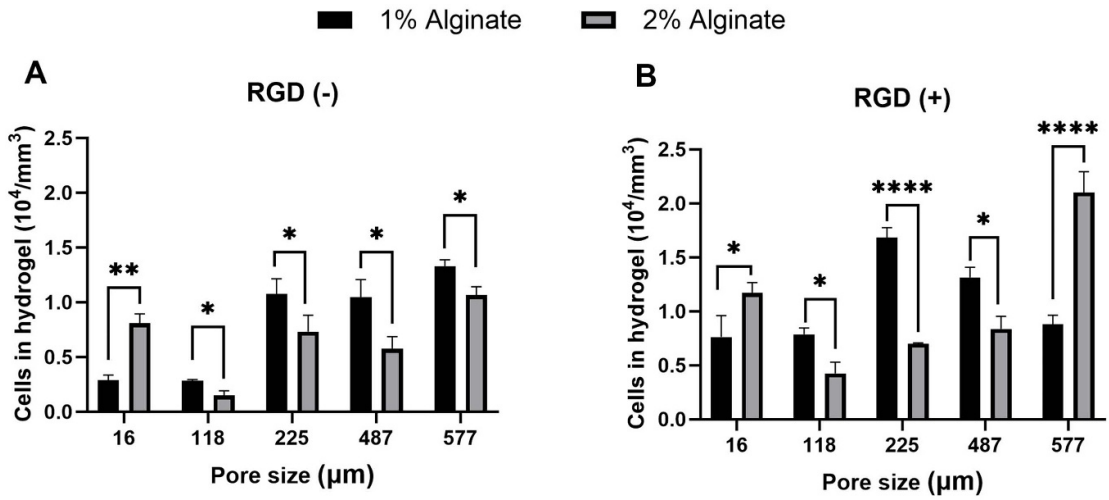

Figure 5. Accumulation of F98 cells expressing the mCherry fluorescent marker in 1% and 2% SA (w/v) hydrogels, with an average pore diameter ranging from 16 to 577 µm (annealing times of PLA molds from 10 to 60 min). The impact of grafting the RGD cell adhesion peptide was also evaluated. $^{*}p < 0.05$, $^{**}p < 0.01$.

cell size, could impede cell colonization. At 1% SA (w/v), approximately 4 times more F98 cells accumulated in hydrogels with an average pore diameter ranging from 225 µm to 577 µm, compared to smaller average pore diameters (from 16 µm to 118 µm) (figure 5(A)). These results confirm that small pore diameters and/or higher tortuosity hinder cell accumulation within the hydrogels. For hydrogels with an average pore diameter of 7 µm, F98 cells remained mostly on the surface (results not shown). Similar trends were observed for 2% w/v SA hydrogels.

On the other hand, increasing the composition in SA from 1% to 2% w/v reduced the accumulation of F98 cells. For example, in hydrogels with an average pore diameter of 225 µm, the accumulation was 1.5 times higher for 1% SA hydrogels, compared to 2% SA. This result could be explained by the negative charge of SA. Since the cell membrane of cancer cells is globally negative, a higher negative surface charge density in 2% SA gels could impede cell adhesion compared to 1% SA.

To promote the accumulation of GBM cells, the RGD cell adhesion peptide was grafted to SA (figure 5(B)). For 1% SA gels, the highest cell accumulation was obtained at the average pore diameter of 225 µm, while the highest accumulation at 2% SA was obtained at 577 µm. Overall, grafting the RDG peptide increased the accumulation of F98 cells by 24% in 1% SA gels, and by 30% in 2% SA gels.

The accumulation of F98 cells was thus affected by the concentration of SA, the average pore diameter, and the presence of the RGD cell adhesion peptide. The best combinations were (1) 1% SA with an average pore diameter of 225 µm, grafted with the RGD peptide, and (2) 2% SA with an average pore diameter of 577 µm, also grafted with the RGD peptide.

3.3.2. Cell retention

The retention of strongly adhered F98 cells was determined next after a more vigorous washing step. For 1% SA (w/v) hydrogels (without RGD), higher retention was obtained at an average pore diameter $\geqslant$ 225 µm (figure 6(A)). On the other hand, at 2% SA, the retention was 2–3 times higher in hydrogels with an average pore diameter of 577 µm (figure 6(B)). The retention was also significantly more important when the average pore diameter was $\geqslant$225 µm, a trend similar to the 1% gels.

Grafting the RGD peptide globally improved the retention of F98 cells in 1% SA hydrogels, with an optimum at 225 µm—except at 577 µm (figure 6(A)). Cell retention was also improved by a factor 2.4 in 1% SA gels with 225 µm pores when grafted with the RGD peptide, compared to the 2% SA gels (also grafted with RGD, figure 6(B)). This suggests that the increased negative surface charge density at 2% SA reduces the efficacity of the RGD peptide to retain the F98 cells. In addition, no significant difference was measured between 2% SA gels with 225 µm pores, grafted or not with the RGD peptide. However, for the 2% SA hydrogels with an average pore size of 577 µm, the unfavorable effect of increasing negative surface charge density on the ability of the RGD peptides to retain the F98 seems attenuated, since 2.3 times more cells were retained in this case compared to 1% SA hydrogels also grafted with RGD.

Overall, the average fraction of F98 cells that were retained in all hydrogels, regardless of average pore size, SA concentration, or presence of RGD, was nearly 83%. The highest accumulation and retention were measured in hydrogels grafted with the RGD adhesion peptide. In 1% SA hydrogels, the most promising pore diameter was 225 µm, and 577 µm for the 2% SA gels.

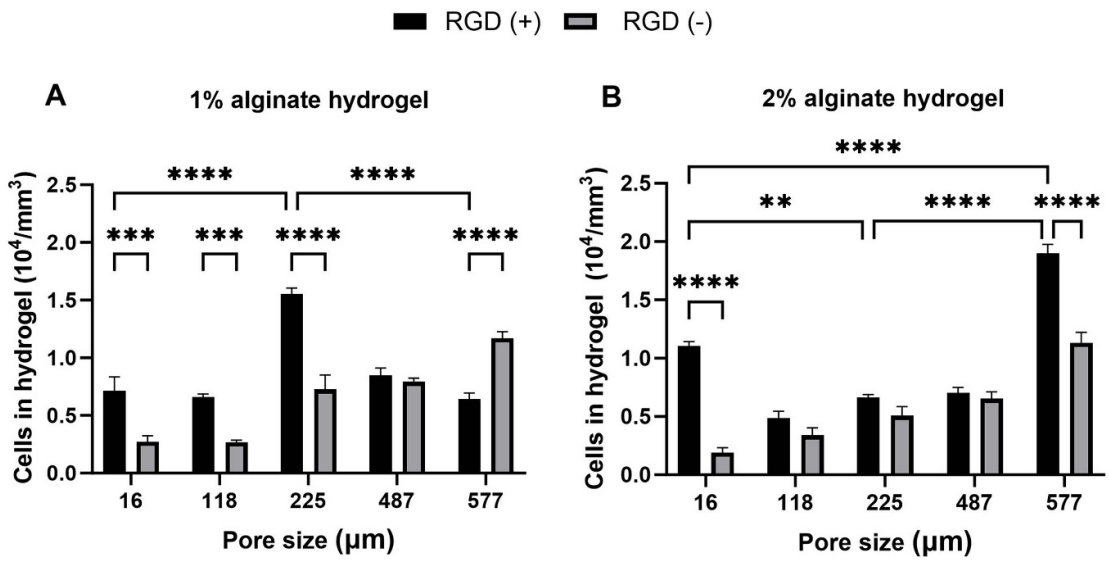

Figure 6. Retention of F98 cells expressing the mCherry fluorescent marker in 1% and 2% SA (w/v) hydrogels, grafted or not with the RGD peptide, with the average pore diameter ranging from 16 to 577 µm. (A) 1% SA hydrogels; (B) 2% SA hydrogels. $^{*}p < 0.05$, $^{**}p < 0.01$.

3.3.3. Cell distribution inside the hydrogels

The distribution of F98 cells within the hydrogels was evaluated as a function of average pore diameter, composition in SA, and presence or not of the RGD adhesion peptide. The F98 cells were fixed 24 h after their addition to the hydrogels, and their distribution in the gels at 5 different levels (denoted L1 to L5), from 1 mm to 4.5 mm deep starting from the top of the gels, was determined using the EVOS FL auto microscope. From the acquired images, the number of cell clusters adhered to the surface of the pores, at each level L, were counted and their size measured. The surface fraction occupied by the F98 cells at each level was also quantified. For example, F98 cell clusters were distributed in levels L1 to L3, at 1% SA (w/v) and at the average pore diameter of 225 µm, when functionalized with the RGD peptide, as figure 7(A)–(C) shows. At a given level, only cell clusters in the focal plane were counted, whereas clusters that were out of focus were not. Figure 7(D) is a magnified view of F98 cell clusters.

The average pore diameter has a significant impact on the distribution of F98 cells across the hydrogels, as determined by the number and mean surface of the cell clusters (figure 8). In 1% SA hydrogels with an average pore size of 16 µm (without RGD), all F98 cells stopped migrating at levels L1 and L2 (figure 8(A)), and the mean surface of cell clusters was larger compared to the results obtained at larger pore sizes (figure 8(B)). By increasing the average pore size to 225 µm and 577 µm, the F98 cells continued to migrate down to level L3, although in progressively fewer numbers. In addition, approximately 1.2 times more cell clusters remained adhered to the hydrogels at an average pore size of 225 µm, compared to 577 µm, but the cell clusters mean surface remained similar. This difference in cell cluster distribution could be the result of both a higher adhesion surface and higher tortuosity as pore size decreases.

The migration of F98 cells throughout the hydrogels was improved by grafting the RGD adhesion peptide (figure 8(C) and (D)). The distribution was limited to levels L1 to L3 in 1% SA hydrogels at an average pore size of 16 µm, grafted with RGD, but extended to levels L4 and L5 for the hydrogels with average pore sizes of 225 and 577 µm. The number of cell clusters also tended to increase by 6–9 times at 225 µm. These results suggest that the higher retention of F98 cells observed by grafting the RGD peptide also improves their distribution in the hydrogels and increases the size of the cell clusters in the deeper layers of the gels (figure 8(D)). The average pore diameter and RGD peptide impacted as well the cell clusters mean surface (figures 8(B) and (D)). At level L1, in the absence of RGD, the highest mean surface value was observed in hydrogels with the smallest average pore size—i.e. 16 µm. This is 1.5 times higher compared to the result obtained for hydrogels with an average pore size of 225 µm. This also suggests that when pore size is too small, the F98 cells do not migrate deep into the hydrogels and therefore remain near the top surface, where they accumulate and thus form larger clusters. When the pore size increases beyond 225 µm, the F98 cells can migrate deeper into the gel where they are retained by the RGD adhesion peptide, which also allows them to form large clusters compared to gels without RGD.

Increasing the concentration of SA from 1% to 2% w/v significantly modifies the distribution of cell

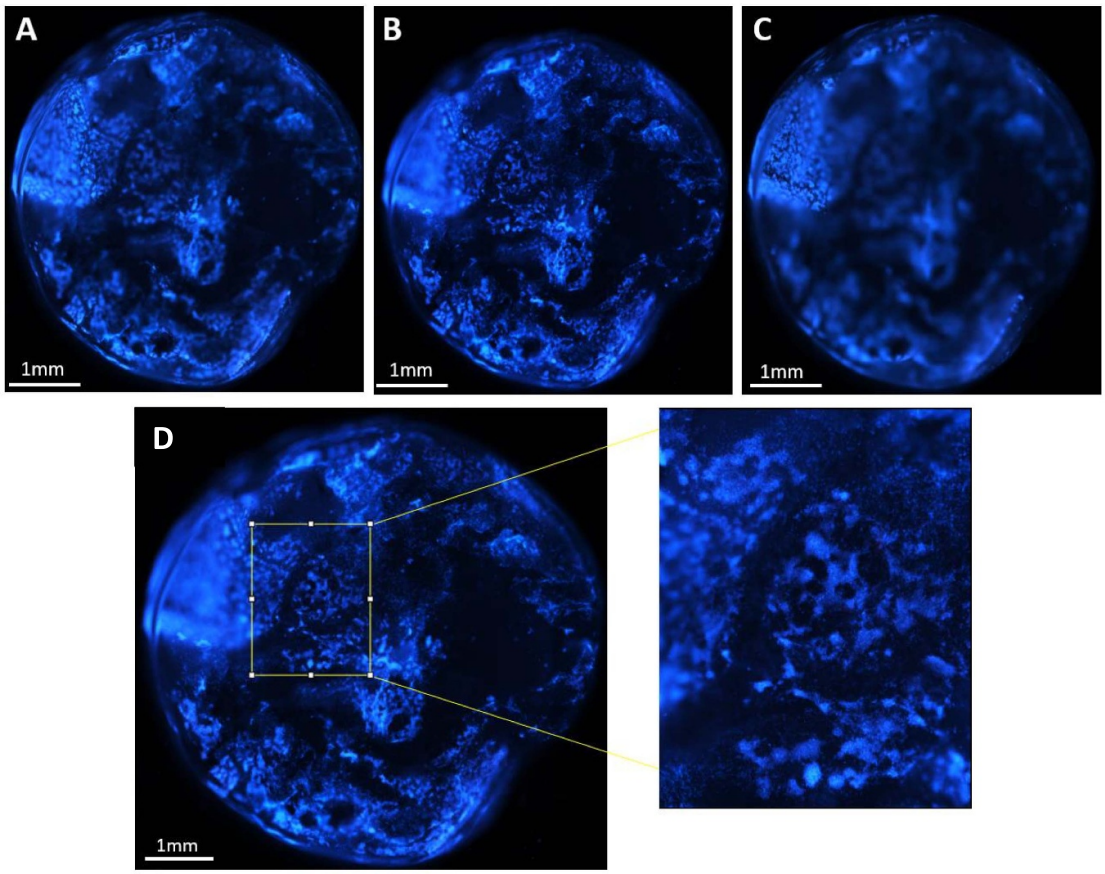

Figure 7. Distribution of F98 cells in a 1% w/v SA gel functionalized with the RGD peptide, at the average pore diameter of 225 μm, observed at levels L1 (A), L2 (B) and L3 (C). 24 h after their addition on the hydrogels, the F98 cells were fixed with PFA and then stained with a mix of Rhodamine-phalloidin 2105 247 and Hoechst 33 342. F98 cells at different levels were observed with the EVOS™ FL Auto Imaging System epifluorescence microscope. In (D), a magnified view of cellular spheroids shown in Level L2 in (B).

clusters (figure 9). At 16 μm, cell clusters (restricted to levels L1 and L2 in 1% SA hydrogels) were observed down to level L3 (figure 9(A), without RGD). At an average pore size of 225 μm, the F98 cells are distributed in all 5 levels (L1 to L5). On the other hand, no F98 cells were observed at levels L1 and L5 when the average pore size reached a value of 577 μm.

Grafting the RGD peptide improved the migration of F98 cells within the 2% SA gels, down to level L5 at 577 μm average pore size (figure 9(C)). At 225 μm, without RGD, the cell clusters average surface was similar for both 1% and 2% SA concentrations (figures 8(B) and 9(B)). For RGD-functionalized hydrogels, the cell clusters mean surfaces were approximately 1.2 times larger in 2% SA hydrogels, compared to 1% SA (figures 8(D) and 9(D)). Overall, grafting the RGD adhesion peptide increased the number of cell clusters and their mean surface. The highest number and mean surface of cell clusters were obtained in 1% SA hydrogels at an average pore size of 225 μm, grafted with the RGD adhesion peptide.

Finally, the surface occupied by the F98 cells in the analyzed micrographs, for both 1% and 2% SA hydrogels, was determined (figure 10). The area fraction occupied by F98 cells reaches a maximum at the average pore size of 225 μm. In particular, the area fraction occupied by F98 cells in 1% SA RGD(+) gels was 4–34 times higher compared to the other two average pore size values (16 μm and 577 μm, 1% SA RGD(+)). It was also 18 times higher compared to the 1% SA RGD(−) gels, 3 times higher compared to the 2% SA RGD(+) hydrogels, and 10 times superior compared to 2% SA RGD(−) gels, for the same average pore size of 225 μm.

4. Discussion

The melt-extrusion technique employed in this work to prepare co-continuous PS/PLA polymer bars, combined with the quiescent annealing treatment and subsequent PS extraction, allows the preparation of porous PLA molds and, ultimately, macroporous hydrogels, with an average pore size ranging from a few microns, to nearly 600 μm (figures 1 and 2). This in turns allows the preparation of significant quantities of porous gels with a large range of average pore sizes, but also of various shapes and sizes necessary for *in vitro* investigations—in this case the effect of pore

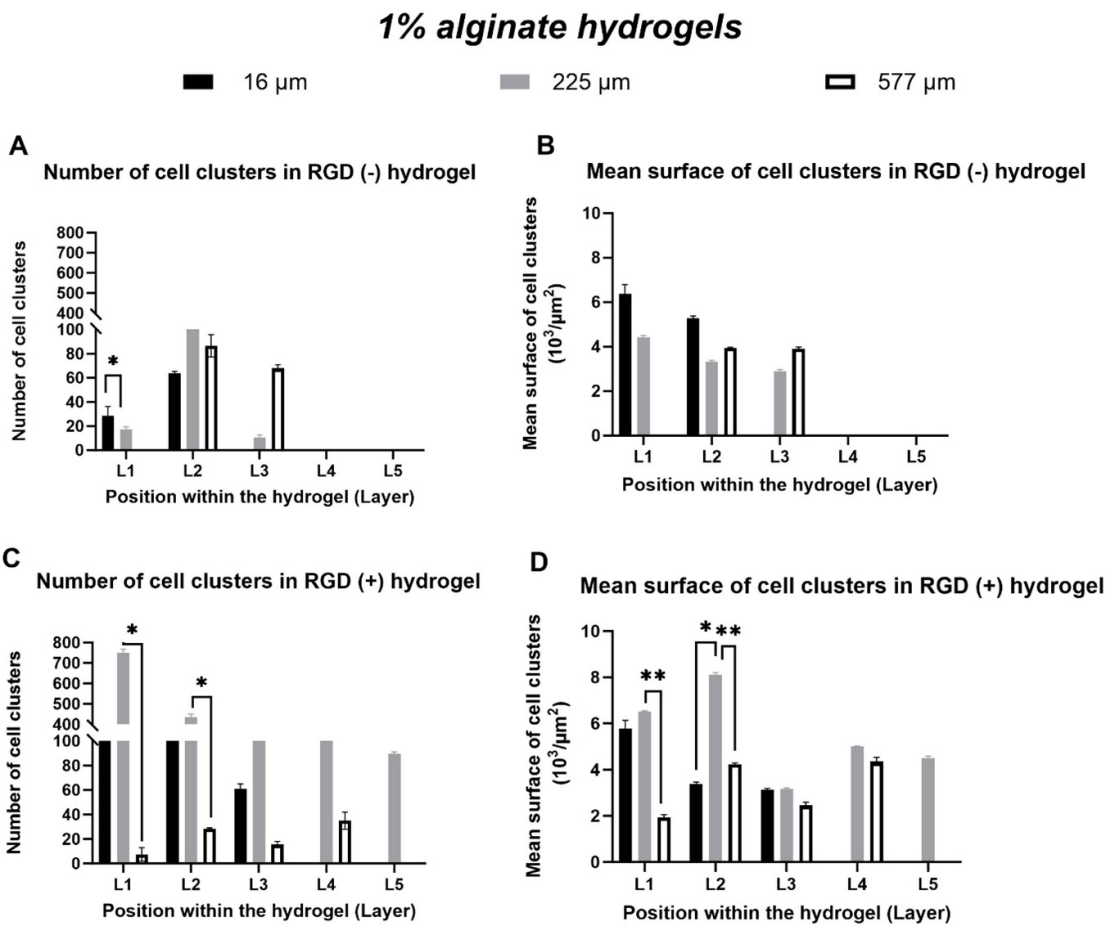

Figure 8. Distribution of F98 cells in 1% macroporous SA hydrogels for 16 µm, 225 µm and 577 µm average pore diameters, and grafted or not with the RGD adhesion peptide. Results are shown for the number of cell clusters (A), (C), and mean surface of cell clusters (B), (D).

size and SA concentration on the mechanical properties, with the added effect of RGD grafting on GBM cell accumulation, retention and distribution within the gels. Although it was not possible to directly compare the morphology of porous gels to the initial PLA molds at small pore sizes, microCT analysis of a gel prepared with a PLA mold initially annealed for 45 min revealed comparable microstructures—i.e. the gels retain the microstructure of the molds once extracted (figure 3).

It is interesting to note next that at a given pore size, doubling the SA concentration roughly doubles the compression modulus value (figure 4)—which is intuitively expected, and verified quantitatively. At 1% SA, for an average pore size equal or superior to 118 µm, the compression modulus is around 15 kPa. Although it is slightly superior to the average value of 1–2 kPa reported for brain tissues [16–18], these hydrogels are still quite soft and constitute a first starting point for a cancer cell trap application, considering that they might have to withstand a certain level of compression induced by the surrounding brain tissues once the tumor is extracted. Furthermore, adding chitosan to the gels, bearing complementary positive charges compared to SA, and chemical crosslinking with natural crosslinkers, such as genipin, should improve gel stability in biological fluids. There is an especially strong effect of pore size on the compression properties for values under 118 µm. More extensive characterization in the future as a function of compression rate, and also under dynamic (oscillatory) conditions, would yield a more thorough understanding on how these materials behave.

The F98 cell accumulation and retention assays clearly reveal that the cells cannot penetrate the hydrogels if the macropores are too small—in our case, below 7 µm. Figure 5(A) shows overall that 1% SA hydrogels better accumulate F98 cells compared to 2% SA hydrogels, and figure 5(B) shows that grafting the RGD peptide also improves accumulation overall. There is, however, an apparent discrepancy since at the average pore diameter of 16 µm, 2% SA gels accumulate more cells than 1% SA gels, without or with the RGD peptides. To explain this apparent discrepancy, we can consider first the average diameter of F98 cells, which is established at about 10 µm

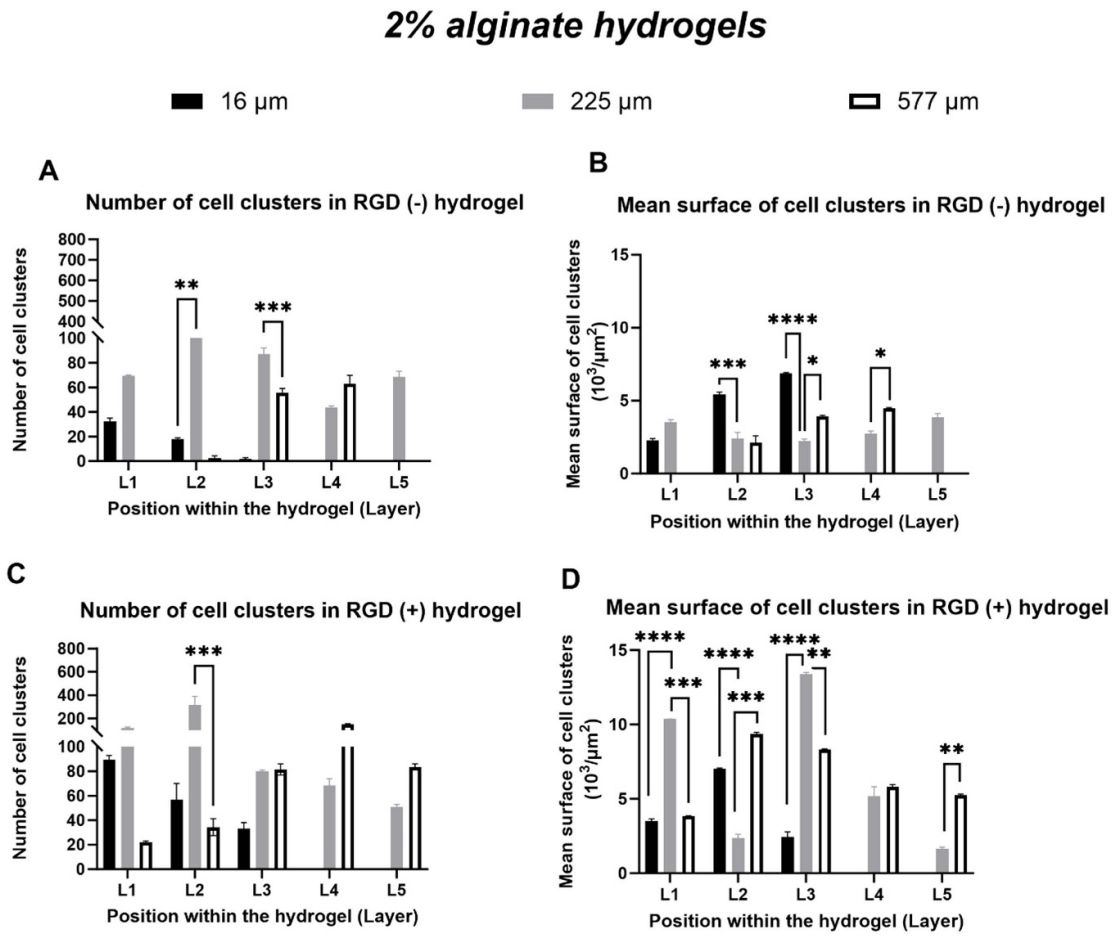

Figure 9. Distribution of F98 cells in macroporous 2% w/v SA hydrogels for 16 µm, 225 µm and 577 µm average pore diameters, and grafted or not with the RGD adhesion peptide. Results are shown for the number of cell clusters (A), (C), and mean surface of cell clusters (B), (D).

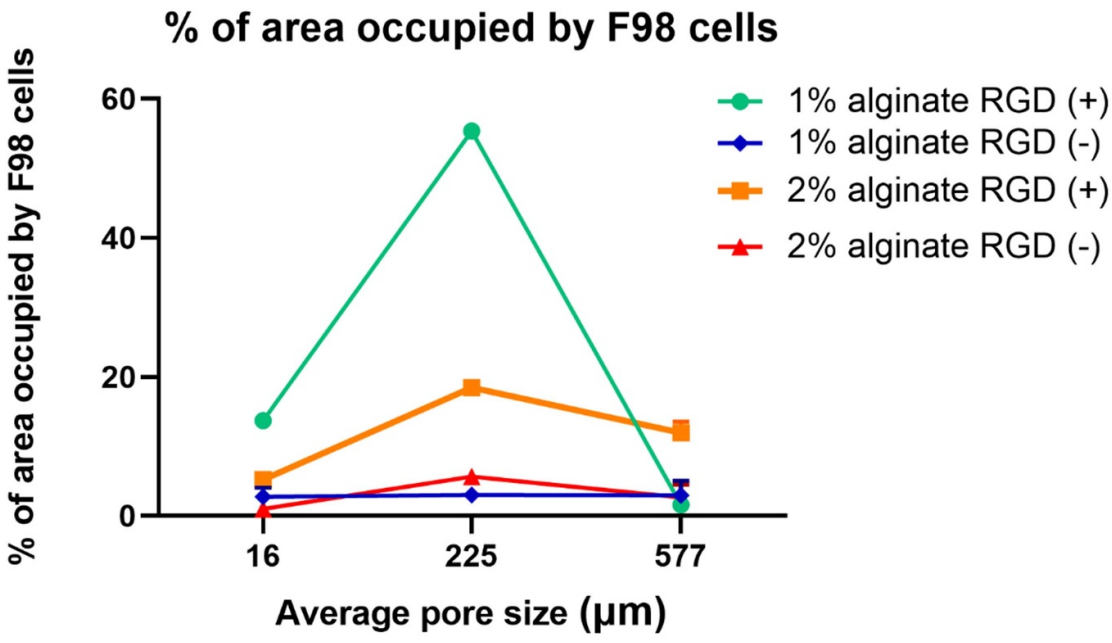

Figure 10. Area fraction (%) occupied by the F98 cells in the gels, in the analyzed micrographs obtained by EVOS microscopy.

[30]. Second, as mentioned earlier, hydrogels with an average pore diameter of 7 μm could not accumulate F98 cells—the pores are smaller compared to the average cell size. At an average pore diameter of 16 μm, slightly superior but still comparable to F98 cell size, cell diffusion is still significantly hindered, up to 118 μm, as figures 5 and 6 show. As expected then, small pores hinder cell diffusion within the hydrogels.

The distribution profiles in figures 8 and 9 provide additional information. At 1% SA (without RGD), F98 cells are only distributed in the first 2 levels (levels 1 and 2, out of a total of 5 levels) near the cell seeding surface, forming relatively large clusters—potentially blocking the lateral pores and pores underneath. Then, increasing the concentration at 2% SA must increase the negative charge at the surface of the pores (sodium alginate is a negatively charged polysaccharide), delaying cell adhesion and promoting their distribution down to level 3, as figure 9 shows, again with the formation of relatively large clusters ultimately blocking the pores down to levels 4 and 5. In short, cell clusters tend to rapidly block small pores, which can be delayed by increasing the surface charge of the gel—i.e. by increasing the SA concentration. As the average pore size increases, pore jamming becomes less significant, and cells can diffuse to deeper levels and in greater numbers, as figures 5, 8 and 9 illustrate, possibly explaining this discrepancy.

In figure 5, at 2% SA (both without and with the RGD peptide), cell accumulation is more important in 16 μm hydrogels compared to 118 μm (not the 1% SA hydrogels, which have cell accumulation capacities that are quite comparable at 16 μm and 118 μm, with and without RGD). In addition, the cells do form clusters near the surface, down to level 3, as the fluorescence microscopy pictures of figure 7 and cell distribution results of figure 9 illustrate. However, pores are more susceptible to be blocked by cell clusters at 16 μm, compared to 118 μm. This unexpected re-increase at 16 μm could be due to a pore jamming issue, with a significant amount of cells trapped in the upper levels—also explaining why retention is higher for this condition, as figure 6(B) shows. This jamming issue is expected to be less pronounced at 118 μm, and in 1% SA gels since they are softer and more deformable.

Cell accumulation and retention within the gels increase once the average pore size reaches 225 μm or more. The distribution of cells within the gel is also more homogeneous throughout the material, especially at 225 μm. Over this value, our results indicate that cells might be able to exit the gels, as there are fewer cells observed in the deepest level observed by microscopy (figures 8 and 9). Overall, our results suggest that the accumulation and retention is optimized at an average pore diameter of 225 μm, at 1% SA functionalized with the RGD peptide (25% to 30% more accumulation, compared to gels without the peptide). This lower SA concentration, while yielding a compression modulus closer to brain tissue properties, will also bear a lower negative surface charge. Combined with the RGD peptide, this could explain why F98 cells, which have an overall negatively charged membrane, are better retained in the 1% SA gels.

Some of the trends observed at the average (and largest) pore diameter of 577 μm are more difficult to interpret, even though these hydrogels accumulate a significant number of F98 cells (down to levels 3–5): (1) at 2% SA, hydrogels grafted with the RGD peptide accumulate more cells compared to 1% SA hydrogels also grafted with RGD (figure 5(B)), contrary to the general trend. (2) At 1% SA, RGD-grafted hydrogels retain fewer F98 cells than pristine hydrogels (without RGD), also contrary to the general and expected trend.

The RDG peptide was grafted at the same ratio for all hydrogels, as described in the Experimental section—its density per pore area remained constant, regardless of pore size. However, the hydrogels display more structural heterogeneities at 577 μm, as figure 2(F) shows. The average pore diameter also becomes more comparable to the hydrogels' dimensions (1 cm × 0.6 cm), with a broad pore size distribution (standard deviation of ±315 μm). Consequently, cells easily diffuse in these hydrogels, but may also easily diffuse out via the lateral and bottom surfaces. In many cases, at 577 μm, no cells are observed at levels 4 and/or 5 in pristine hydrogels, whereas grafting the RGD peptide increases the number of cells observed at levels 4 and 5, as figures 8 and 9 show. As such, it is possible that a microstructural limit is reached in terms of the average pore diameter/gel dimensions ratio, and the capacity of these hydrogels to retain F98 cells efficiently.

In a previous work, SA/chitosan (CHI) macroporous gels comprising interconnected 600 μm pores also accumulated F98 GBM cells in the whole volume of the gels [14]. Combined with CHI, grafting the RGD cell-adhesion peptides to SA resulted in 100% increase in accumulated F98 cells (which overexpress the associated $\alpha v\beta 3$ and $\alpha v\beta 5$ binding integrins) retained in the gels. However, while the RGD peptide clearly improved the accumulation and retention of GBM cells, the addition of both RGD and CHI, also known to promote cell adhesion, led to significant GBM cell proliferation—an undesired feature. In that case, using only CHI, without the RGD peptide, resulted in both improved accumulation and retention of GBM cells, with limited proliferation. In the present work, the RGD adhesion peptide also promoted cell adhesion and retention, with similar limited proliferation—providing

different and complementary pathways to gradually tune and optimize the required material, cell accumulation and retention properties.

In this work, we needed a high throughput fabrication technique allowing us to tune relatively precisely the average pore size of the hydrogels, while maintaining full pore interconnectivity. Melt-extrusion followed by thermal annealing of the material allowed both. However, the random character/orientation of the hydrogels' microstructure and resulting porosity, combined with the challenge of counting and establishing the distribution of cells in 3D materials, probably explains some of the variability observed in the results. This limit is probably exacerbated when the average pore size reaches 500 µm—a scale at which the average pore size is only about 10 times smaller than the dimensions of the gels.

Future work will assess which chemokines, gradually liberated from the hydrogels, can attract GBM cells into the pores for a variety of GBM cell lines. In an *in vivo* context, healthy cells are also expected to migrate within the hydrogels. Implanting the hydrogel into the brain will induce an inflammatory response that will attract microglial cells, the most important immune cells in the brain, as well as immune cells, such as T lymphocytes, from the bloodstream. These immune cells, combined with radiotherapy, are expected to contribute to the elimination of cancer cells trapped in the hydrogels.

5. Conclusion

This work evaluates the capacity of GBM cells to penetrate and accumulate in 3D porous hydrogels with full pore interconnectivity, as a function of pore size and mechanical compression modulus. Such data remain scarce in the literature in general for cells, but are necessary to design and fabricate efficient porous 3D scaffolds. This work demonstrates that in order to efficiently accumulate and retain GBM brain cancer cells within a macroporous sodium alginate-based hydrogel trap, a new therapeutic paradigm currently under development to treat GBM, the pores must have an average pore size superior to 100 µm, with the best results obtained at 225 µm. At this average pore size value, the accumulation and retention of GBM cells was more homogeneous throughout the gels, especially when functionalized with RGD adhesion peptides. Below 100 µm, cell penetration within the hydrogels is significantly hindered, whereas no cells are observed in the hydrogels below an average pore size of 10 µm. On the other end of the spectrum, over 500 µm, pore size and heterogeneities due to the fabrication process become comparable in size to the hydrogels, probably causing variability issues in the results. In addition, at an alginate concentration of 1% w/v, the compression modulus was around 15 kPa, which is relatively close to the range of 1–2 kPa values reported for brain tissues.

The porous gels were prepared with porous polylactide molds obtained from an extruded co-continuous blend of polystyrene and polylactide, treated by quiescent annealing, in order to tune the morphology of the molds. This technique allows for the preparation of a significant quantity of macroporous gels of various sizes, shapes, and compositions, with an average pore size ranging from nearly 5 µm, to over 500 µm—offering the possibility to assess the effect of pore size on 3D cell culture assays over two orders of magnitude. Whether these results translate directly *in vivo* will be addressed in a future work.

Data availability statement

All data that support the findings of this study are included within the article (and any supplementary files).

Acknowledgments

The authors thank Dr Marie-Hélène Bernier, from the GCM laboratory, for her expertise and support with the MicroCT experiments (Polytechnique Montreal).

Author contributions

The manuscript was written through contributions of all authors. All authors have given approval to the final version of the manuscript.

Funding Sources

The authors acknowledge the *Fonds de Recherche du Québec—Nature et Technologie* for financial support via the *Projet de Recherche en Équipe* program (grant number 2022-PR-299713), as well as the *New Frontiers in Research—Exploration* program. This work was also supported by the TransMedTech Institute (NanoBio Technology Platform) and its main funding partner, the Canada First Research Excellence Fund. N. Virgilio acknowledges the financial support of Polytechnique Montréal via the UPIR program.

ORCID iD

Nick Virgilio https://orcid.org/0000-0002-5629-4867

References

[1] Mohammed S, Dinesan M and Ajayakumar T 2022 Survival and quality of life analysis in glioblastoma multiforme with adjuvant chemoradiotherapy: a retrospective study *Rep. Pract. Oncol. Radiother.* **27** 1026–36

[2] Wen P Y *et al* 2020 Glioblastoma in adults: a Society for Neuro-Oncology (SNO) and European Society of Neuro-Oncology (EANO) consensus review on current management and future directions *Neuro Oncol.* **22** 1073–113

[3] Ostrom Q T, Cioffi G, Gittleman H, Patil N, Waite K, Kruchko C and Barnholtz-Sloan J S 2019 CBTRUS statistical report: primary brain and other central nervous system tumors diagnosed in the United States in 2012–2016 *Neuro Oncol.* **21** V1–V100
[4] Fayzullin A, Sandberg C J, Spreadbury M, Saberniak B M, Grieg Z, Skaga E, Langmoen I A and Vik-Mo E O 2019 Phenotypic and expressional heterogeneity in the invasive glioma cells *Transl. Oncol.* **12** 122–33
[5] Hanif F, Muzaffar K, Perveen K, Malhi S M and Simjee S U 2017 Glioblastoma multiforme: a review of its epidemiology and pathogenesis through clinical presentation and treatment *Asian Pac. J. Cancer Prev.* **18** 3–9
[6] Drean A, Goldwirt L, Verreault M, Canney M, Schmitt C, Guehennec J, Delattre J Y, Carpentier A and Idbaih A 2016 Blood-brain barrier, cytotoxic chemotherapies and glioblastoma *Expert Rev. Neurother.* **16** 1285–300
[7] D'Alessandris Q G *et al* 2017 The clinical value of patient-derived glioblastoma tumorspheres in predicting treatment response *Neuro Oncol.* **19** 1097–108
[8] Stupp R *et al* 2005 Radiotherapy plus concomitant and adjuvant temozolomide for glioblastoma *New Engl. J. Med.* **352** 987–96
[9] Solanki C, Sadana D, Arimappamagan A, Rao K, Rajeswaran J, Subbakrishna D K, Santosh V and Pandey P 2017 Impairments in quality of life and cognitive functions in long-term survivors of glioblastoma *J. Neurosci. Rural Pract.* **8** 228–35
[10] Ashby L S, Smith K A and Stea B 2016 Gliadel wafer implantation combined with standard radiotherapy and concurrent followed by adjuvant temozolomide for treatment of newly diagnosed high-grade glioma: a systematic literature review *World J. Surg. Oncol.* **14** 15
[11] Champeaux C and Weller J 2020 Implantation of carmustine wafers (Gliadel (R)) for high-grade glioma treatment. A 9-year nationwide retrospective study *J. Neuro-Oncol.* **147** 159–69
[12] Rong L, Li N and Zhang Z Z 2022 Emerging therapies for glioblastoma: current state and future directions *J. Exp. Clin. Cancer Res.* **41** 18
[13] Autier L, Clavreul A, Cacicedo M L, Franconi F, Sindji L, Rousseau A, Perrot R, Montero-Menei C N, Castro G R and Menei P 2019 A new glioblastoma cell trap for implantation after surgical resection *Acta Biomater.* **84** 268–79
[14] Safi C *et al* 2022 Effect of chitosan on alginate-based macroporous hydrogels for the capture of glioblastoma cancer cells *ACS Appl. Bio Mater.* **5** 4531–40
[15] Solano A G, Dupuy J, Therriault H, Liberelle B, Faucheux N, Lauzon M A, Virgilio N and Paquette B 2021 An alginate-based macroporous hydrogel matrix to trap cancer cells *Carbohydrate Polym.* **266** 118115
[16] Rashid B, Destrade M and Gilchrist M D 2012 Mechanical characterization of brain tissue in compression at dynamic strain rates *J. Mech. Behav. Biomed. Mater.* **10** 23–38
[17] Budday S, Nay R, de Rooij R, Steinmann P, Wyrobek T, Ovaert T C and Kuhl E 2015 Mechanical properties of gray and white matter brain tissue by indentation *J. Mech. Behav. Biomed. Mater.* **46** 318–30
[18] Murphy A R, Laslett A, O'Brien C M and Cameron N R 2017 Scaffolds for 3D in vitro culture of neural lineage cells *Acta Biomater.* **54** 1–20
[19] Esquirol A-L, Sarazin P and Virgilio N 2014 Tunable porous hydrogels from cocontinuous polymer blends *Macromolecules* **47** 3068–75
[20] Oliverio R, Patenaude V, Liberelle B, Virgilio N, Banquy X and De Crescenzo G 2022 Macroporous dextran hydrogels for controlled growth factor capture and delivery using coiled-coil interactions *Acta Biomater.* **153** 190–203
[21] Chiu Y C, Cheng M H, Engel H, Kao S W, Larson J C, Gupta S and Brey E M 2011 The role of pore size on vascularization and tissue remodeling in PEG hydrogels *Biomaterials* **32** 6045–51
[22] Lo C M, Wang H B, Dembo M and Wang Y L 2000 Cell movement is guided by the rigidity of the substrate *Biophys. J.* **79** 144–52
[23] Wang H B, Dembo M, Hanks S K and Wang Y L 2001 Focal adhesion kinase is involved in mechanosensing during fibroblast migration *Proc. Natl Acad. Sci. USA* **98** 11295–300
[24] Lang N R, Skodzek K, Hurst S, Mainka A, Steinwachs J, Schneider J, Aifantis K E and Fabry B 2015 Biphasic response of cell invasion to matrix stiffness in three-dimensional biopolymer networks *Acta Biomater.* **13** 61–67
[25] Bouchard G, Bouvette G, Therriault H, Bujold R, Saucier C and Paquette B 2013 Pre-irradiation of mouse mammary gland stimulates cancer cell migration and development of lung metastases *Br. J. Cancer* **109** 1829–38
[26] Lopez-Barron C R and Macosko C W 2009 Coarsening of PS/SAN blends with cocontinuous morphology studied with 3D image analysis *Macromol. Symp.* **283–284** 348–53
[27] Lopez-Barron C R and Macosko C W 2010 A new model for the coarsening of cocontinuous morphologies *Soft Matter* **6** 2637–47
[28] Virgilio N, Desjardins P, L'Esperance G and Favis B D 2009 In situ measure of interfacial tensions in ternary and quaternary immiscible polymer blends demonstrating partial wetting *Macromolecules* **42** 7518–29
[29] Zhang R Z, Chen J, Zhu Y X, Zhang J, Luo G Q, Cao P, Shen Q and Zhang L M 2020 Correlation between the structure and compressive property of PMMA microcellular foams fabricated by supercritical CO_2 foaming method *Polymers* **12** 315
[30] Hoa N *et al* 2010 Glioma cells display complex cell surface topographies that resist the actions of cytolytic effector lymphocytes *J. Immunol.* **185** 4793–803